Anal. Bioanal. Electrochem., Vol. 17, No. 6, 2025, 428-445
https://www.doi.org/10.22034/abec.2025.725947

Analytical & Bioanalytical Electrochemistry

www.abechem.com

Full Paper

Eco-Friendly Green Synthesis of Reduced Graphene Oxide as An Electrocatalytic Platform for The Simultaneous Detection of Cd(II) and Pb(II)

Thu Huong Nguyen ,[1,2] Tieu My Pham,[1,2] and Minh Huy Do[1,2]

[1]*Department of Analytical Chemistry, Faculty of Chemistry, University of Science, Ho Chi Minh City, 227 Nguyen Van Cu, District 5, Ho Chi Minh City, 70000, Vietnam*
[2]*Vietnam national university, Ho Chi Minh city, Linh Trung ward, Thu Duc city, Ho Chi Minh city, 70000, Vietnam*

*Corresponding Author, Tel.: +84-899-899-702
E-Mail: domhuy@hcmus.edu.vn

Received: 10 April 2025 / Received in revised form: 31 May 2025 / Accepted: 20 June 2025 / Published online: 7 July 2025

Abstract- A sensitive and reliable technique for monitoring lead and cadmium using a reduced graphene oxide-modified glassy carbon electrode (rGO/GCE) and a wireless potentiostat has been developed. In this study, rGO was synthesized employing green tea extract as a reducing and stabilizing agent. The initial glassy carbon electrode was electrochemically activated in a 0.5 mol L-1 nitric acid solution and then coated with rGO by the drop-casting method, which increased the effective surface area and enhanced sensitivity. The rGO-modified glassy carbon electrode was employed to quantify Cd(II) and Pb(II) in an acetate buffer at pH 5 using differential pulse voltammetry. Under optimal conditions, the peak currents of Cd(II) and Pb(II) exhibited good linear relationships with their concentrations in the ranges of 2.4 to 12.5 µmol L^{-1} for Cd(II) and 1.5 to 6.8 µmol L^{-1} for Pb(II), with detection limits of 1.1 µmol L^{-1} and 0.88 µmol L^{-1}, respectively. The rGO/GCE was applied to analyze metal ions in simulated battery samples, demonstrating reliability and accuracy comparable to atomic absorption spectroscopy.

Keywords- Cadmium; Lead; Reduced graphene oxide; Green tea; Green synthesis

1. INTRODUCTION

Heavy metal pollution in the environment has become a global issue due to industrial and agricultural activities, as well as uncontrolled emissions from various waste sources. Among heavy metals, lead and cadmium are particularly toxic elements, capable of accumulating in ecosystems and causing severe health consequences [1]. Meanwhile, the global generation of electronic waste is estimated to reach 49.8 million metric tons per year and is one of the fastest-growing waste streams, with an annual growth rate of 8% [2]. The rapid increase in e-waste, driven by the short lifespan of electronic products, has heightened the risk of pollution from heavy metals present in printed circuit boards and electronic components. Therefore, the analysis and monitoring of heavy metal concentrations, particularly lead and cadmium, in e-waste play a crucial role in protecting the environment, human health, and sustainable development towards a net-zero waste treatment technology [3]. These toxic metals, commonly found in spent batteries, pose severe risks to ecosystems and human health due to their persistence and bioaccumulation potential. Accurate detection and quantification of Pb(II) and Cd(II) enable effective pollution monitoring, risk assessment, and waste management strategies. By identifying contamination levels, appropriate recycling and remediation processes can be implemented, reducing the release of hazardous substances into the environment. Furthermore, extracting and reusing these metals from battery waste decreases the demand for primary mining, thereby lowering carbon emissions associated with raw material extraction and refining.

Several analytical techniques have been employed to identify these metal contaminants, such as atomic absorption spectrophotometry [4-6], ICP-MS) [7], ICP-OES [8], and ICP-AES [9]. However, the main challenge remains in developing methods that require complex sample preparation, are time-consuming, and are not suitable for field measurements. Due to its sensitivity, low operational cost, and suitability for real-time, on-site analysis, voltammetry has emerged as a valuable analytical approach. Kokkinos and colleagues developed disposable bismuth-based microelectrode arrays designed for stripping voltammetric analysis of trace metals, demonstrating effective Pb(II) and Cd(II) analysis in static solutions [10]. In a recent review, Holmes discussed key developments in trace metal voltammetry, noting the growing adoption of bismuth film and screen-printed electrodes for Pb(II) and Cd(II) analysis due to their improved sensitivity and reduced toxicity relative to mercury electrodes [11]. Other studies have focused on integrating microfluidic paper-based analytical devices with boron-doped diamond paste electrodes, allowing for sensitive detection of Pb(II) and Cd(II) at concentrations as low as a few micrograms per liter. These findings suggest that voltammetric techniques, particularly those utilizing environmentally friendly electrode materials, continue to evolve as promising alternatives for Pb(II) and Cd(II) analysis in complex matrices [12].

A key aspect in improving the efficiency of voltammetric techniques lies in selecting suitable materials for electrode surface modification. Among these, reduced graphene oxide

(rGO) has gained widespread interest since its introduction, particularly in electrochemical research, due to its outstanding electrical characteristics. Electrodes modified with rGO have attracted attention in electroanalytical applications for their high conductivity, large active surface area, and facile functionalization. Several reduction methods are available to convert graphene oxide (GO) into rGO, including chemical, electrochemical, hydrothermal, solvothermal, photochemical, thermal, and multi-step reduction processes involving different reducing agents. However, these conventional methods come with notable drawbacks, such as poor control over the final product, complex multi-step procedures, high energy consumption, and the release of hazardous chemicals that pose environmental risks [13].

Recently, the use of plant-based reducing agents, such as aloe vera and green tea extracts, has gained increasing attention [14]. This green chemistry approach avoids the use of toxic chemicals, positioning itself as a sustainable and eco-friendly alternative to conventional chemical reduction processes for rGO production. Among these methods, green tea extract has demonstrated significant potential as a reducing agent. It contains polyphenols, particularly catechins, which effectively reduce GO to rGO while introducing oxygen-containing functional groups that enhance metal ion binding [15].

This study aims to combine green synthesis of rGO using green tea extract with electrochemical activation of GCE and wireless potentiostat-based voltammetric detection, creating a sensitive, eco-friendly, and portable platform for monitoring Cd(II) and Pb(II) in battery-related samples. This approach offers a novel integration of sustainability and practical applicability for heavy metal detection in electronic waste contexts.

2. EXPERIMENTAL SECTION

2.1. Chemicals and reagents

Cd(II) 1000 mg L^{-1} (Merck, Certipur), Pb(II) 1000 mg L^{-1} (Merck, Certipur), graphene oxide (GO) flakes (15–20 layers) were purchased from Sigma-Aldrich, potassium hexacyanoferrate (II) trihydrate (Scharlau, purity ≥ 99.0%), potassium hexacyanoferrate (III) (Merck, ≥ 99.0%), potassium, chloride (Merck, 99.5%), sodium acetate (Merck, ≥ 99.0%), sodium sulfate (Merck, ≥ 99.0%), sodium hydroxide (Merck, ≥ 85%), potassium dihydrogen phosphate (Merck, ≥ 99.5%), di-potassium hydrogen phosphate trihydrate (Merck, ≥ 99.0%), sodium chloride (Guangdong Guanghua Chemical, ≥ 99.0%), potassium nitrate (Merck, ≥ 99.0%), nitric acid 85% (Merck), boric acid (Scharlau, ≥ 99.5%), sulfuric acid 95-97% (Merck), and ortho-phosphoric acid 85% (Scharlau). Ethanol and methanol were obtained from Scharlau (Spain).

2.2. Instrumentation

Differential pulse voltametric (DPV) measurements were conducted using a compact finger-sized potentiostat-Zensor/ECWP100 (Taiwan) in a three-electrode configuration: an

Ag/AgCl/KCl 3 M reference electrode (YB481 ALS RE-1B, OD = 6 mm, L = 78 mm), a glassy carbon working electrode (ALS, ID = 3 mm, OD = 6 mm, L = 55 mm), and a platinum rod auxiliary electrode. pH measurements of buffer solutions were carried out with a Mettler Toledo Basic S749 Seven Excellence system pH electrode (Mettler Toledo, USA). The characterization of GO, rGO, and green tea extract was measured by employing UV-1800 Shimadzu spectrometer (Japan), FTIR spectrophotometer (6600 type A JASCO, Japan). X-ray diffraction (XRD) analysis was conducted using a D8 Advance Eco XRD system (Germany) operating at 40 kV, 25 mA, with Cu Kα radiation at a wavelength of 0.154 nm. Electron microscopic analysis was utilized using Field-emission scanning electron microscopy (FE-SEM, Merlin Compact, Carl Zeiss, Jena, Germany). The analysis was performed at a 5kV accelerating voltage, and the sample was coated with a thin conducting platinum layer using a sputter coater (Quorum Q150T, Quorum Technologies, East Sussex, UK) prior to analysis.

2.3. Fabrication of rGO/GCE electrode for analysis

2.3.1. Green tea extract preparation

A 3 g sample of Tan Cuong green tea (Vietnam) was placed in a 250 mL beaker and mixed with 150 mL of distilled water. The mixture was heated to 60 ºC for 30 minutes in a water bath. The solution was then allowed to cool to room temperature and transferred into centrifuge tubes, where it was centrifuged at 2000 rpm for 10 minutes. The supernatant was filtered through Newstar 102 filter paper (20 µm pore size) in a Buchner funnel to obtain the green tea extract. The extract was stored in a tube at 4 °C, wrapped in silver paper to protect it from light exposure. Before use, the tea extract was vigorously shaken, allowed to reach room temperature, and then subjected to ultrasonication for approximately 30 min.

2.3.2. Synthesis of reduced graphene oxide

To prepare a 0.5 mg/mL GO solution, 10.0 mg of GO was weighed and added to 20 mL of deionized water, followed by ultrasonication to ensure thorough dispersion.

rGO was synthesized by adding 10 mL of diluted green tea extract dropwise to 20 mL of 0.5 mg/mL GO solution over 45 minutes and heating at 60ºC for 6 hours [16]. The mixture was centrifuged at 3000 rpm for 20 minutes, washed three times with water, and dried at 70°C for 24 hours.

2.3.3. Fabrication of rGO/GCE electrode for analysis

To eliminate adsorbed impurities and residues from previous measurements, the GCE surface was polished using 1 µm aluminum oxide powder suspension (Lake Bluff-IL-USA) on a polishing pad. Subsequently, the electrode surface was polished 20 times in figure-eight motion on a polishing pad without using the aluminum oxide powder. Following the polishing process, the electrode underwent ultrasonic treatment using ethanol for 3 min, rinsed with ultra-

pure water. After being thoroughly cleaned, GCE has activated electrochemically pretreatment through a pretreatment process as previously reported [17,18]. The electrode was immersed in a 0.5 mol/L nitric acid solution and subjected to cyclic voltammetry (CV) from -0.20 V to +1.60 V at 100 mV/s for 30 cycles. To prepare rGO/GCE, 5 µL of 10 mg mL^{-1} rGO solution was drop-cast onto the GCE and dried at room temperature.

2.3.4. Electrochemical measurements

For the electrochemical characterization of the composite, a CV experiment was conducted at 100 mV s^{-1} within the potential range of -1500 mV to -200 mV. DPV measurements were recorded in a 0.1 mol L^{-1} suitable buffer, within a potential range of -1500 mV to -200 mV, with pulse width 200 ms at a pulse amplitude of 50 mV, containing 20.0 mL of Cd(II) (4.5×10^{-6} µmol L^{-1}) and Pb(II) (2.4×10^{-6} µmol L^{-1}). The measurements were conducted at room temperature.

2.4. Sample preparation

2.4.1. Sample preparation for total polyphenol analysis by spectrophotometry method

The total phenolic content was performed by the spectrophotometry method using the Folin-Ciocalteu method according to TCVN 9745-1:2013 [19]. A 0.2 g sample was weighed into a 100 mL beaker, and 25 mL of methanol:water (7:3) solution was added. The mixture was heated at 70 ºC for 30 minutes, followed by centrifugation at 6000 rpm for 5 minutes. The supernatant was collected, and extraction was repeated with the residue. The combined extracts were diluted to 100 mL with ultrapure water. A 2 mL aliquot of the extract was reacted with 5 mL of 10% Folin-Ciocalteu reagent for 5 minutes. Subsequently, 4 mL of 7.5% sodium carbonate solution was added. After incubation at room temperature for 1 hour, absorbance at 756 nm was measured using a UV-Vis 1800 Spectrophotometer (Shimadzu, Japan). A calibration curve was generated using gallic acid. All analyses were performed in triplicate.

2.4.2. Sample preparation for polyphenol analysis by HPLC-UV

To analyze polyphenols by HPLC-UV, 0.2 g of tea was extracted with 25 mL of methanol:water (7:3) at 70ºC for 30 minutes. After centrifugation, the supernatant was collected, and the extraction was repeated. The extracts were combined, diluted to 10 mL with ultrapure water, and filtered through a 0.45 µm membrane. The filtered solution was then ready for HPLC-UV analysis.

2.4.3. Sample preparation for cadmium and lead analysis in battery simulation solutions by DPV using rGO/GCE

The battery sample composition was simulated based on the solution obtained after the cathode was hydrolyzed using acid, which contained Co, Li, Mn, and Ni [20]. The solution has a pH of 7 with ion concentrations of 0.17 mmol L^{-1} Co(II), 1.4 mmol L^{-1} Li(I), 0.13 mmol L^{-1}

Mn(II), and 0.53 mmol L^{-1} Ni(II). Prior to analysis 200 μL of simulated battery sample was diluted one hundred-fold with 0.1 M acetate buffer (pH 5). Then, add standard Pb(II) and Cd(II) solutions, and the concentration of target ions was analyzed by the standard addition method.

3. RESULTS AND DISCUSSION

3.1. Characterization of GO, rGO materials, and green tea extract

3.1.1. Polyphenol in green tea extract

The total polyphenol content of the tea extract, determined by the Folin-Ciocalteu method, was 111.13 ± 0.04 mg g^{-1}, accounting for 11.1% of the tea composition. The high polyphenol content suggests a strong reducing potential, which is crucial for the green reduction of GO to rGO.

HPLC-UV analysis identified epigallocatechin gallate (EGCG) as the most abundant polyphenol (7.74%), followed by epicatechin (EC, 2.83%), epicatechin gallate (ECG, 1.52%), epigallocatechin (EGC, 1.33%), and (+)-catechin (0.5%). These catechins, particularly EGCG, are known for their redox properties, playing a key role in the reduction process of GO. The presence of multiple hydroxyl groups in these compounds facilitates electron transfer, promoting the conversion of GO to rGO while potentially enhancing the stability and functional properties of the resulting material.

UV-VIS absorption peaks of green tea extract are characterized by two main absorption peaks located at 270 nm and 330 nm. T. Atomssa's study also proved the spectra of catechins in water and methanol ranged from 246 nm to 323 nm [21]. In the infrared spectrum of green tea, the band at 3440 cm^{-1} corresponds to the stretching vibration of the O–H group in water, alcohols, and phenols, as well as the N–H stretching compression in amines. The C–H stretching vibration in alkanes and the O–H stretching vibration in carboxylic acids appear at 2926 and 2800 cm^{-1}, respectively. The strong band at 1660 cm^{-1} is attributed to the C=C stretching vibration in aromatic rings and the C=O stretch in polyphenols. The C–O–C stretch in polysaccharides produces a band, and the C–O–C stretch in amino acids generates a band at 1030 cm^{-1}. These spectral characteristics indicate that the green tea sample is rich in polyphenols, carboxylic acids, polysaccharides, amino acids, and proteins.

3.1.2. Characterization of GO, rGO materials

To evaluate the efficiency of rGO) synthesis, UV-Vis spectroscopy was utilized to analyze the properties of GO and rGO solutions. As shown in Figure 1a**,** the spectroscopic data reveal a distinct shift in absorption peaks. GO exhibited a peak at 230 nm, while rGO displayed a peak at 270 nm. These results are consistent with findings reported by Elham Vatandost and colleagues. The absorption peak at 230 nm for GO corresponds to $\pi \rightarrow \pi^*$ electron transitions within the graphitic C-C bonds. In contrast, the redshift to 270 nm in rGO is due to the restoration of electronic conjugation and the π–π^* transition of the graphitic C–C rings [22].

A comparative FT-IR spectroscopic analysis of GO and rGO is presented in Figure 1b. In the FT-IR spectrum of GO, a broad absorption peak at 3387 cm^{-1} corresponds to the stretching vibration of hydroxyl groups (O-H). Additionally, a band at 1601 cm^{-1} is attributed to the symmetrical stretching vibrations of C=O in carboxyl groups (–COOH), while the stretching vibration of C-O-C (epoxy group) appears at 1049 cm^{-1}. In contrast, the FT-IR spectrum of rGO exhibits a narrower and less intense peak at approximately 3400 cm^{-1}, indicating a significant reduction in hydroxyl groups. Furthermore, the C=O peak at 1692 cm^{-1} exhibits a significant decrease in intensity compared to the corresponding peak in GO, indicating the removal of oxygenated groups during the reduction process. The overall attenuation of oxygen-containing functional peaks in the FT-IR spectrum of rGO further supports the successful conversion of GO to rGO.

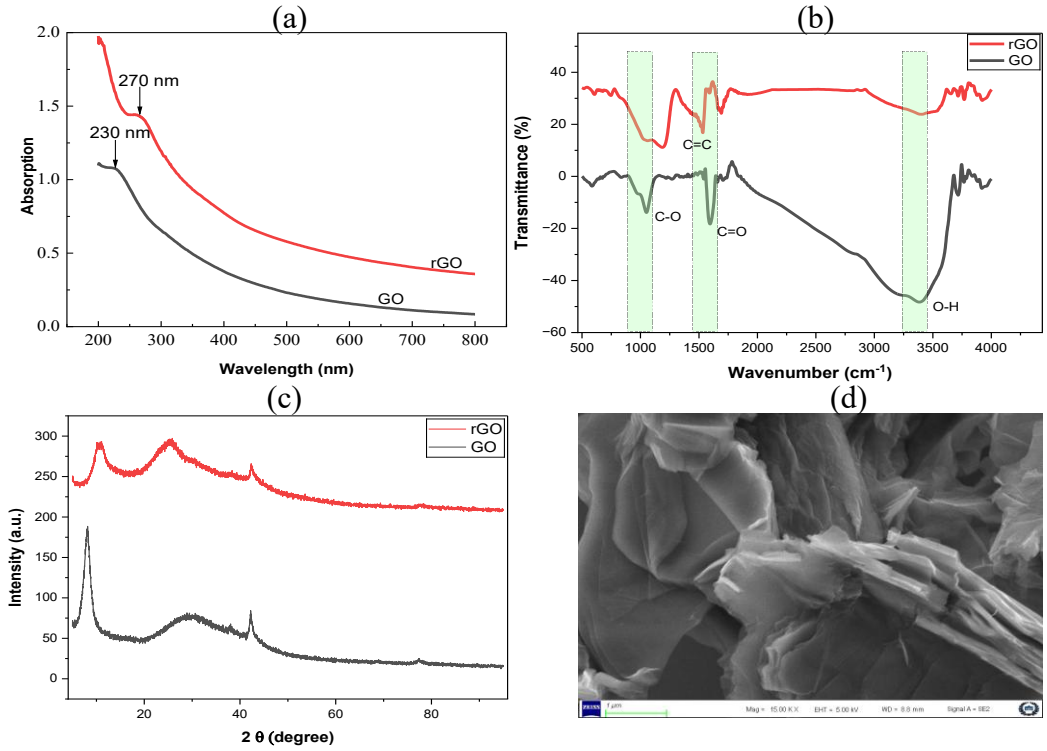

Figure 1. Physicochemical characterization of the GO and synthesized rGO material: (a) UV-Vis, (b) FTIR, (c) XRD pattern, (d) and FE-SEM image of rGO

The formation of rGO was further confirmed using SEM and XRD. The XRD patterns of GO and rGO are presented in Figure 1c. Due to the presence of oxygen-containing functional groups and atomic-scale roughness arising from structural defects (sp^2 bonding) in the originally flat graphene sheet, GO exhibited a d-spacing of approximately 0.76 nm ($2\theta \approx 11.7°$). Upon reduction with green tea extract, the GO peak gradually disappeared, and a broad diffraction peak emerged between 24° and 29°, corresponding to a d-spacing of approximately 0.35 nm. This reduction in interlayer spacing suggests that rGO has a more compact structure

than GO. The decrease in interlayer distance reflects the removal of oxygen-containing functional groups and the restoration of the conjugated sp^2 carbon network during the reduction process, including the ring-opening of epoxy groups. These findings confirm the successful reduction of GO to rGO using green tea extract.

The surface morphology of the rGO was examined using FE-SEM. At 1500× magnification shown in Figure 1d, the rGO material comprises thin, well-defined sheets stacked in a layered structure. This characteristic arrangement, along with observable exfoliation, enhances the material's porosity. Additionally, the wrinkled surfaces and folds increase the effective surface area, facilitating improved molecular interactions. These structural features highlight the potential of rGO for applications requiring high surface area and enhanced molecular interactions.

3.1. Electrochemical characterization of GO/GCE and rGO/GCE surfaces

Cyclic voltammetric profiles of $Fe(CN)_6^{4-/3-}$ in 0.1 M KCl at various electrodes were illustrated in Figure 2a. A comparison of the electrochemical signals of ($Fe(CN)_6^{4-/3-}$) on two types of modified electrodes reveals that the rGO/GCE electrode (81.2 μA) exhibits a significantly higher signal intensity than the GO/GCE electrode (62.7 μA). This difference is attributed to the presence of oxygen-containing functional groups in the GO structure, which occupy interlayer positions and disrupt the sp^2 network. As a result, GO has poor electrical conductivity, limiting electron transfer between analytes and the GO/GCE-modified electrode surface, thereby leading to a lower measured current. In contrast, the reduction of GO to rGO removes these oxygen-containing groups, enhancing the electrical conductivity of the modified material and consequently improving the current intensity.

The cyclic voltammetry method at different scan rate (ν) measuring the 5.0×10^{-3} mol L^{-1} $Fe(CN)_6^{-3/-4}$ in 0.10 mol L^{-1} KCl used to compare electrochemical activity between GO/GCE and rGO/GCE. The linear standard curves of the current at different scan rates I_p *vs.* $\nu^{1/2}$ were plotted based on the Randles-Sevcik equation (Figure 2b**)**.

$$I_p = \pm(2.69\times10^{6.5})\, n^{3/2} A\, D^{1/2}\, C\, \vartheta^{1/2}$$

I_p: the cathodic peak current,
n: the number of electrons transferred,
A_0: the surface area of the electrode,
D_0: the diffusion coefficient,
V: the scan rate and C_0: the concentration of $K_3Fe(CN)_6^{-3/-4}$.

The effective surface areas of the rGO/GCE and GO/GCE electrodes were calculated to be 0.025 cm^2 and 0.008 cm^2, respectively. These values demonstrate that the rGO/GCE electrode has a surface area three times greater than that of the GO/GCE electrode. This increase in

surface area suggests that rGO/GCE enhances the overall performance of the modified electrode by providing more active sites for electrochemical reactions.

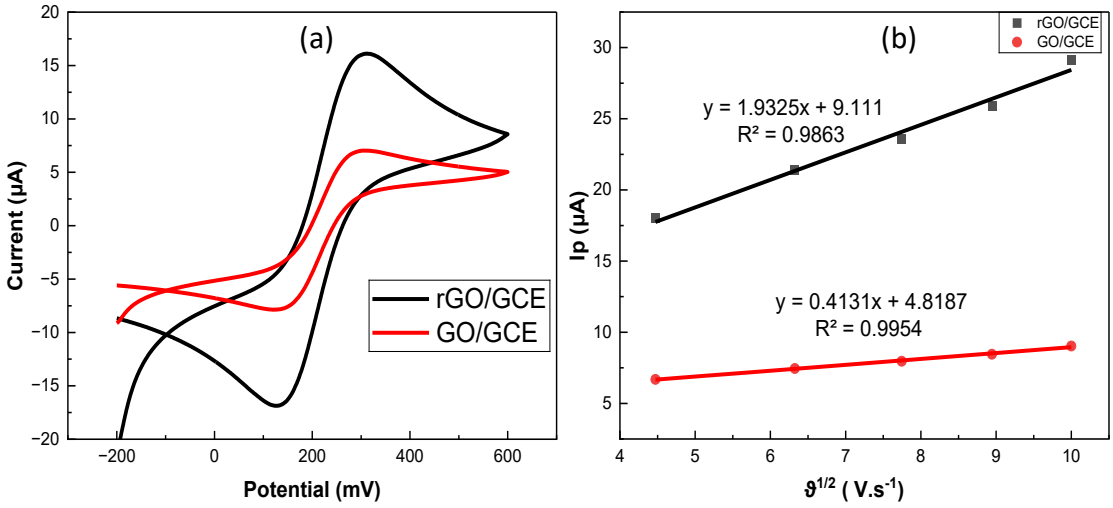

Figure 2. (a) Cyclic voltammograms of 5.0 mol L^{-1} $Fe(CN)^{3-/4-}$ in 0.1 mol L^{-1} KCl at GCE, GO/GCE, and rGO/GCE (b) The linear sweep voltammetry current-voltage curves based on the Randles-Sevcik equation for the measurement process of $Fe(CN)_6^{3-/4-}$ on the electrodes

3.2. Electrochemical behavior for cadmium and lead at rGO/GCE

The electrochemical behavior of Cd(II) and Pb(II) on rGO/GCE was investigated using CV DPV. As shown in Figure 3a, distinct oxidation peaks were observed at approximately -820 mV for Cd(II) and -610 mV for Pb(II), confirming the effective electrochemical activity of the modified electrode. Similarly, DPV results (Figure 3b) showed oxidation peaks at -830 mV for Cd(II) and -610 mV for Pb(II), consistent with previous findings by Vasanthi and colleagues [23].

A significant increase in oxidation peak current was observed for rGO/GCE compared to GO/GCE, while no redox peaks were detected on bare GCE, indicating that the presence of graphene-based materials is crucial for the electrochemical detection of these metal ions. Notably, the peak currents for Pb(II) on rGO/GCE were approximately three times higher than those on GO/GCE, highlighting the superior conductivity of rGO. This enhancement can be attributed to the substantial reduction of oxygen-containing functional groups on rGO, which facilitates electron transfer and improves the electrode's overall electrochemical performance.

The improved sensitivity and reproducibility of rGO/GCE suggest its strong potential for detecting trace levels of Cd(II) and Pb(II) in environmental and industrial samples. The well-defined peaks with minimal background noise further indicate that rGO provides a stable and effective platform for electrochemical sensing. Compared to GO/GCE, the enhanced performance of rGO/GCE underscores the importance of surface chemistry and conductivity in designing advanced electrochemical sensors for heavy metal detection.

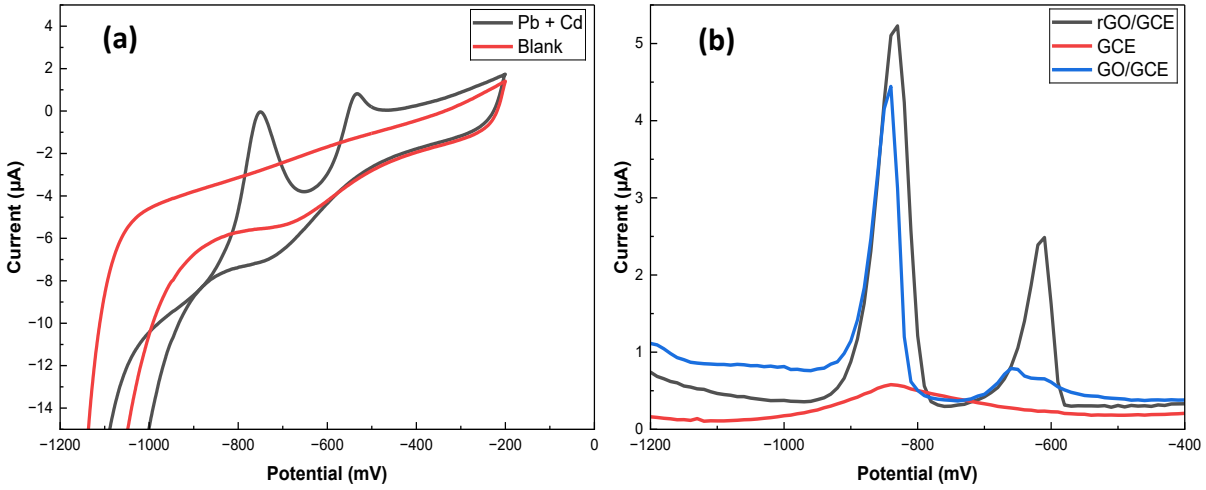

Figure 3. Cyclic voltammogram (a) and differential pulse voltammograms (b) recorded at electrodes in the presence of Cd(II) (2.4×10^{-6} µmol L^{-1}) and Pb(II) (4.5×10^{-6} µmol L^{-1}) in sodium acetate (pH 5.0)

3.3. Optimization of experimental conditions

3.4.1. Effect of rGO volume and adsorption time

The influence of rGO volume coated on the GCE electrode was evaluated based on the signal intensity of Pb(II) and Cd(II) at rGO volumes of 4 µL, 5 µL, and 6 µL. As shown in Figure 4a, the rGO volume had a significant impact on the signal response. Increasing the rGO volume from 4 µL to 5 µL resulted in an enhanced signal. However, when the volume exceeded 5 µL, the I_{pa} signal decreased sharply, with a 60% reduction for Pb and a 10% reduction for Cd.

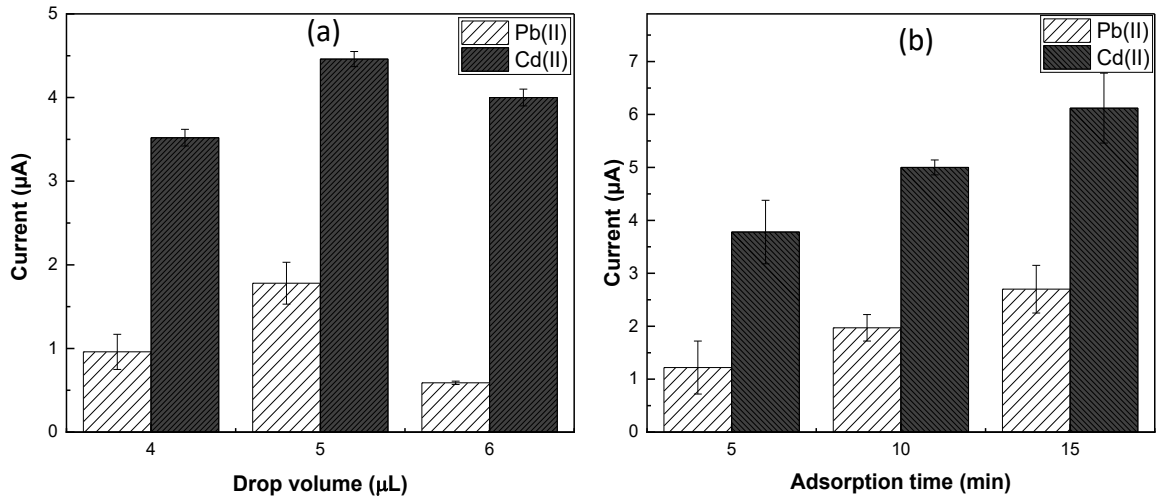

Figure 4. The effect of (a) drop volume and (b) absorption time of 2.4 µmol L^{-1} Cd (II) and 4.5 µmol L^{-1} Pb (II) in electrolyte solution (pH 5.0)

At volumes below 5 µL, the incomplete coverage of the GCE surface reduces the effective surface area and catalytic efficiency. In contrast, at volumes above 5 µL, the increased film thickness raises charge transfer resistance, hindering electron transport. The significant decline in the Pb signal, due to lower sensitivity, highlights its susceptibility to charge transfer resistance. Additionally, excessive material spreading at higher volumes further decreases the effective rGO coverage. Therefore, 5 µL is identified as the optimal volume for further studies.

Similarly, as depicted in Figure 4b, increasing adsorption time enhances signal intensity; however, prolonged adsorption reduces stability. The high standard deviation observed at 10 minutes is attributed to the diminished durability of rGO on the GCE surface, leading to instability across measurements. Conversely, 5 minutes is insufficient for effective metal adsorption and stable signal response. As a result, an adsorption time of 10 minutes was chosen as the optimal condition for subsequent analysis.

3.4.2. Optimization of electrode operating conditions

To obtain the best voltammetric responses for heavy metal detection, it is crucial to optimize several experimental parameters, including pH, electrolyte composition, pulse width, pulse amplitude, and pulse increment. Previous studies have demonstrated that pH is a crucial parameter influencing the quantification of metal ions [24,25]. In this study, pH medium was investigated in the range of 2–7 (data not shown). The response peaks of both Cd(II) and Pb(II) exhibited relatively high intensity and achieved stability at pH 5. This result is consistent with several previous studies. As a result, pH 5 was chosen to study the effect of buffer composition on the measurement signal. Figure 5a illustrates that the current intensity for both Pb(II) and Cd(II) was highest when using an acetate buffer. Therefore, a 0.1 M acetate buffer at pH 5 was selected for subsequent investigations.

Pulse amplitude significantly influences the current intensity of the analyte. A small pulse amplitude results in a low current intensity, whereas a large pulse amplitude leads to a higher current intensity. However, an excessive pulse amplitude causes peak broadening and potential drift, and affecting quantification accuracy in real sample. As the results in Figure 5b, the pulse amplitude increases from 20 mV to 100 mV, the DPV voltammogram shows a gradual rise in the signal intensity of Pb(II) and Cd(II). However, at pulse amplitudes higher than 50mV, the baseline also rises significantly, causing peak broadening and reducing both selectivity and resolution. It is observed that pulse amplitude values of 20 mV and 50 mV provide signals with a signal stability for both Pb(II) and Cd(II) (RSD 15% and 4%, respectively). Based on these observations, 50 mV is identified as the optimal pulse amplitude for further analysis. Pulse width was evaluated based on the signal intensity and repeatability for Pb(II) and Cd(II) solutions at values of 100 ms, 200 ms, 300 ms, and 400 ms.

Figure 5c indicates that as pulse width increases from 100 ms to 400 ms, the DPV voltammogram progressively shifts downward, the reduction peaks of Pb(II) and Cd(II) broaden, and the current intensity decreases. At a pulse width 100 ms, the signal exhibits

significant noise, making it difficult to determine accurate values, thereby reducing sensitivity and precision. At pulse width 200 ms, Cd(II) achieves the highest current intensity (2.29 μA) with an RSD of 17% while the current intensity of Pb(II) is lower than at a pulse width of 300 ms (0.8 vs. 1.1 μA), although the RSD values at pulse width 200 ms and 300 ms are similar (17% and 18%, respectively). Considering both metals, the pulse width of 200 ms is selected as the optimal condition, as it provides high sensitivity, well-defined peaks, minimal noise, and good repeatability for both Pb(II) and Cd(II).

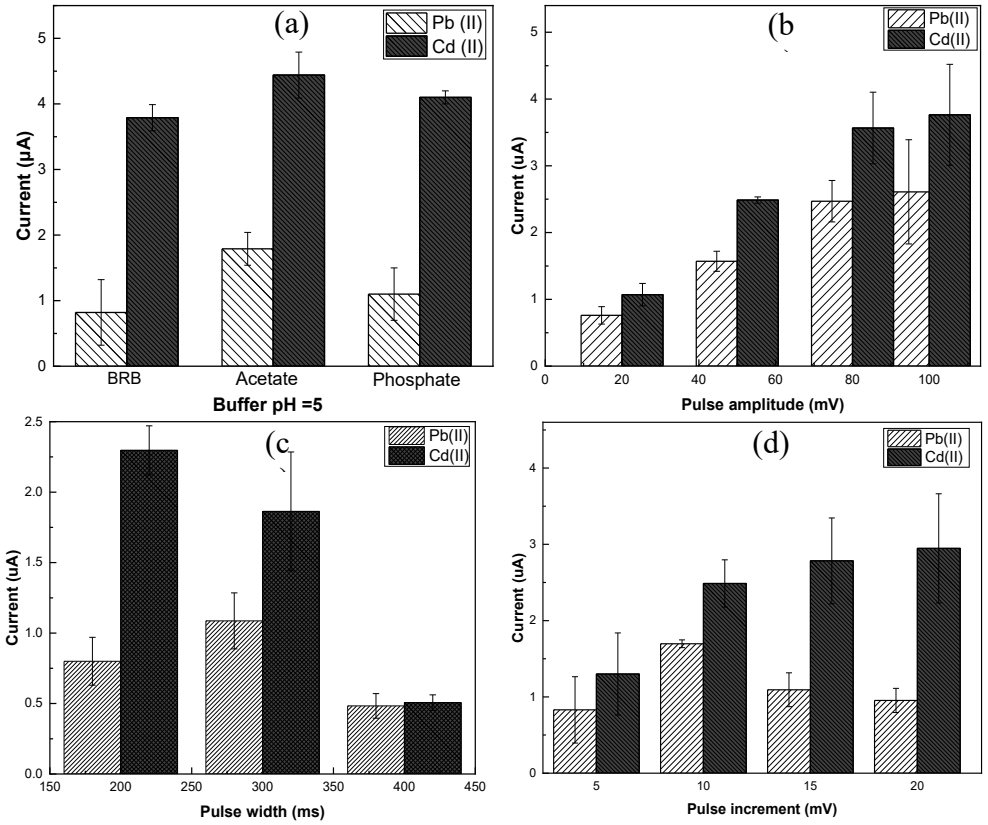

Figure 5. Optimized pH and DPV parameters for the simultaneous determination of cadmium and lead ions using the rGO/GCE

Pulse increment was evaluated based on the current intensity and repeatability of Pb(II) and Cd(II) signals at values of 5 mV, 10 mV, 15 mV, and 20 mV. Results from Figure 5d show that as the pulse increment increases from 10 mV to 20 mV, the DPV voltammogram shifts upward, reduction peaks become more distinct, and current intensity increases with pulse increment. In contrast, at pulse increment 5 mV, the signal is significantly lower. Pulse increment 10 mV provided the highest Pb(II) signal (1.69 μA) with the lowest RSD (5%). For Cd(II), the difference in current intensity between these two values was negligible (2.41 μA *vs.* 2.74 μA), but the RSD at pulse increment 10 mV was lower than at pulse increment 15 mV. Since pulse

increment does not substantially impact current intensity, the key consideration is that a pulse increment 10 mV produces sharper peaks, enhances sensitivity, and minimizes baseline elevation. Therefore, a pulse increment 10 mV was selected as the optimal value. Table 1 summarizes the optimal parameters.

Table 1. Optimization parameters of DPV using rGO/GCE to detect Cd(II) and Pb(II)

Parameters	**Optimize value**
Electrolyte solution	Acetate buffer, pH 5
Method	DPV
Initial potential	-1500 mV
Final potential	-200 mV
Pulse amplitude	50 mV
Pulse width	200 ms
Pulse increment	10 mV

3.4. Linear range and performance of the method

DPV technique was employed for the quantification of Pb(II) and Cd(II) under optimized experimental conditions. Figure 6 demonstrates a progressive increase in oxidation peak currents with increasing Pb(II) and Cd(II) concentrations. The calculated LOD and LOQ for Pb(II) were 1.1 µmol L^{-1} and 3.3 µmol L^{-1}, respectively [26]. Similarly, for Cd(II), the LOD and LOQ were determined to be 0.88 µmol L^{-1} and 2.6 µmol L^{-1}, respectively.

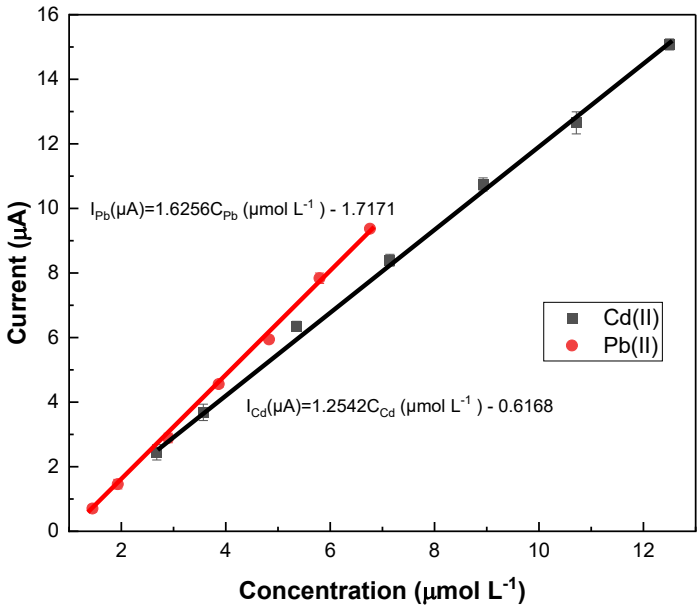

Figure 6. Calibration plots for Pb(II) and Cd(II) in 0.1 M acetate buffer at pH 5

Compared to previous studies related to electroanalytical methods for Pb(II) and Cd(II) detection, the proposed method in this study exhibited good analytical performance in terms of LOD and working range (Table 2).

The reproducibility of the activated GCE was evaluated by performing six consecutive determinations of 2.4 μmol L^{-1} Cd(II) and 4.5 μmol L^{-1} Pb(II). After each determination, the used electrode undergoes a new surface modification process with rGO. The measurements demonstrated good reproducibility, with a relative standard deviation (RSD) of 3.8% for Pb and 3.9% for Cd(II). The DPV response for six measurements at the same rGO/GCE for Pb(II) and Cd(II) with the RSD was about 3.6%.

These values comply with AOAC criteria, which require RSDs in the range of 16–22% at concentrations in the μg L^{-1} level. Therefore, the repeatability of the method is sufficient for the simultaneous quantification of Pb(II) and Cd(II).

Table 2. Evaluation of the proposed method against existing electroanalytical approaches for Pb(II) and Cd(II) detection

Working electrode	Technique	Sample	LODs μmol L^{-1}		Ref.
			Cd	Pb	
Cyclodextrin/CPE	DPASV	Standard solutions	2.0	0.60	[27]
CPE/MBT	DPASV	River water	1.7	63	[28]
Co3O4/GO	DPASV	Real water	0.57	0.29	[29]
rGO/Sb/GCE	SWASV	Chamomile tea	0.70	0.45	[30]
rGO/aGCE	DPV	Stimulated baterry	1.1	0.88	This study

DPASV: Differential Pulse Stripping Voltammetry
SWASV: Square Wave Anodic Stripping Voltammetry

3.5. Study of interferences

In order to develop an analytical method for the determination of Pb(II) and Cd(II) in electronic waste using DPV, a study was undertaken to examine the influence of common interfering ions on the electrochemical responses of Pb(II) and Cd(II). The interfering ions were introduced at concentrations three times greater than those of the target ions. The electrochemical signals of Pb(II) and Cd(II) were subsequently measured under the optimal experimental conditions. The results indicated that most interfering ions slightly reduced the signals of Pb(II) and Cd(II) due to the competition among cations for adsorption on the negatively charged surface of rGO (Figure 7). Notably, Fe(III) induced a significant decrease in signal intensity, attributed to its high charge and strong electrostatic interactions with the

oxidized functional groups of rGO. Although both Fe(III) and Cr(III) possess a +3 charge, Fe(III) has a larger ionic radius, resulting in a higher charge density and, consequently, a greater adsorption affinity for the rGO surface. This preferential adsorption of Fe(III) reduces competition for adsorption sites in the Pb(II) and Cd(II) analysis solution [31,32]. Regarding common anions (SO_4^{2-}, NO_3^-, Cl^-), no significant effect was observed, as these negatively charged species do not interact with the remaining oxygen functional groups on rGO and not induce surface competition with metal ions.

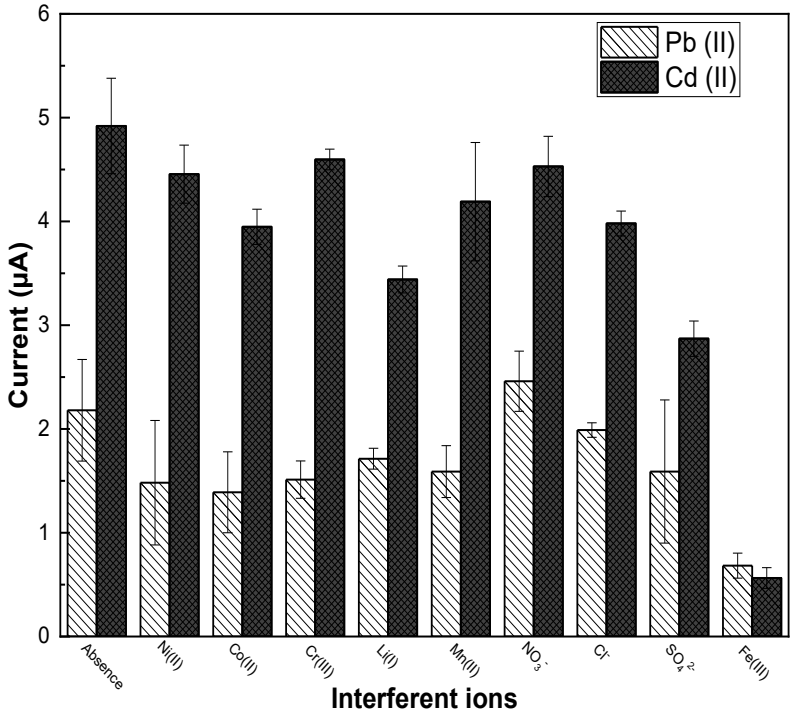

Figure 7. Current respond of individual metal ions in the presence and absence of interfering ions with a 1:3 concentration ratio of analyte to interfering ions

3.6. Sample analysis

To further assess the analytical reliability and practical applicability of this electrochemical assay, it was applied to determine Pb(II) and Cd(II) in battery simulation solutions using the standard addition method. Each sample was analyzed in triplicate by standard addition method (Figure 8). The accuracy of electrochemical analysis was compared with atomic absorption spectroscopy (AAS) in determining Pb and Cd concentrations in an electronic waste sample. A paired t-test showed no significant difference between the two methods. The calculated t-values for Pb(II) ($t = 0.598$) and Cd(II) ($t = 0.664$) were both lower than the critical t-value ($t = 4.303$) at $p = 0.05$, indicating comparable accuracy. This suggests that the modified electrodes offer reliable detection of Cd(II) and Pb(II) in complex matrices, making them suitable for real sample analysis.

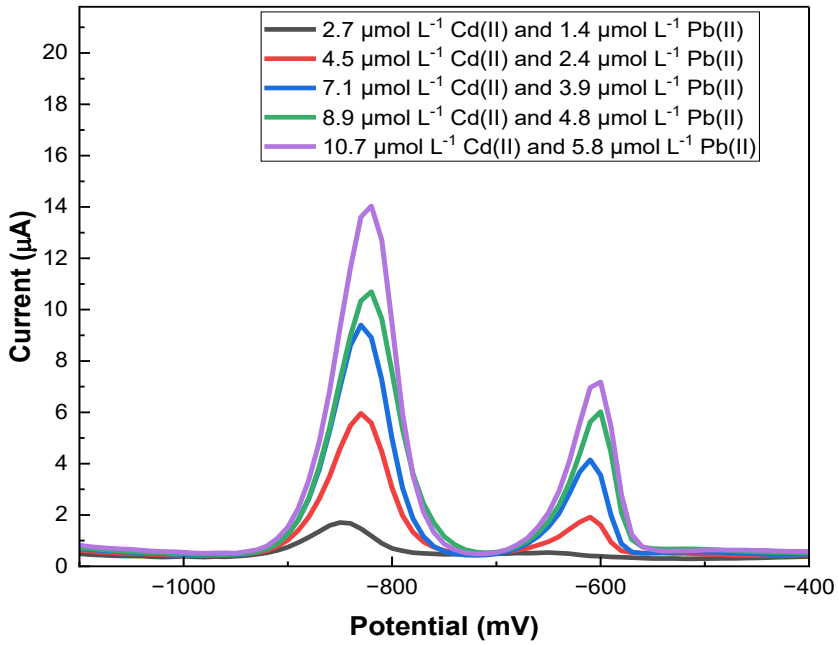

Figure 8. Differential pulse voltammograms of battery simulation sample and four standard additions of cadmium and lead

Table 3. Analysis results of Pb(II) and Cd(II) concentrations using the electrochemical method and the atomic absorption sepcctroscopy method

Metal ions	Method	Concentration (µmol L^{-1})
Cd(II)	DPV	7.777±0.031
	AAS	7.791±0.039
Pb(II)	DPV	14.40±0.074
	AAS	14.69±0.024

4. CONCLUSION

In conclusion, this study demonstrates the development of a sensitive and reliable technique for monitoring lead and cadmium using a rGO/GCE coupled with a wireless potentiostat. The rGO modification significantly enhanced the electrode's surface area and sensitivity, enabling accurate quantification of Cd(II) and Pb(II) in acetate buffer. The method showed a good linear relationship between oxidation peak currents and concentrations of the metal ions, with low detection limits for both Pb(II) and Cd(II). Furthermore, the rGO/GCE exhibited reliability and accuracy in analyzing metal ions in simulated battery samples, showing performance comparable to atomic absorption spectroscopy. This approach provides a promising alternative for environmental monitoring and real sample analysis of hazardous metal ions. In future studies, we plan to investigate the potential interference of additional heavy metal ions,

including Hg(II), to broaden the applicability of the sensor system to more complex or legacy e-waste matrices.

Acknowledgments

This research is funded by the University of Science, Vietnam National University, Ho Chi Minh City, under grant number T2023-35. The authors are grateful for the financial support of the University of Science.

Declarations of interest

The authors declare no conflict of interest in this reported work.

REFERENCES

[1] Alengebawy, S.T. Abdelkhalek, S.R. Qureshi, and M.Q. Wang, Toxics 9 (2021) 42.
[2] O. Osibanjo, and I.C. Nnorom, in: M.A. Azevedo (Ed.), Metal Sustainability, Elsevier, Amsterdam (2016) pp. 52–84.
[3] S. Mao, Y. Zhang, L. Cao, Y. Lu, and Y. Luo, Chemosphere 245 (2020) 125645.
[4] M. Solchaga, R. Montoro, and M. De La Guardia, J. Assoc. Off. Anal. Chem. 69 (1986) 874.
[5] B.K. Bansod, T. Kumar, R. Thakur, S. Rana, and I. Singh, Biosens. Bioelectron. 94 (2017) 443.
[6] T. Daşbaşı, Ş. Kartal, L. Elçi, and M. Soylak, Food Chem. 203 (2016) 283.
[7] J. Koelmel, and D. Amarasriwardena, Environ. Pollut. 168 (2012) 62.
[8] A.M. Massadeh, I.F. Al-Momani, and R.M. Haddad, Environ. Sci. Pollut. Res. 23 (2016) 13424.
[9] K. Sreenivasa Rao, T. Balaji, T. Prasada Rao, and G.R.K. Naidu, Spectrochim. Acta B 57 (2002) 1333.
[10] Kokkinos, A. Economou, M.I. Prodromidis, and C.E. Efstathiou, Electrochem. Commun. 13 (2011) 391.
[11] J.C. Holmes, P. Pathirathna, and P. Hashemi, TrAC Trends Anal. Chem. 111 (2019) 206.
[12] S. Nantaphol, O. Chailapakul, and W. Siangproh, Anal. Chem. 89 (2017) 4100.
[13] X. Gao, J. Jang, and S. Nagase, J. Phys. Chem. C 114 (2010) 832.
[14] A.A. Moosa, and J. Jaafar, Nanoscience Nanotechnol. 7 (2017) 38.
[15] H. Incebay, L. Aktepe, and Z. Leblebici, Surf. Interfaces 21 (2020) 100726.
[16] W. Grosse, E. Ehrentreich-Förster, and F.W. Scheller, Carbon 61 (2013) 467.
[17] N.T. Huong, N.T. M.H. Hien, T.T.D. Thuy, N.T. N. Ai, and L.D.Q. Anh, Vietnam J. Chem. 61 (2023) 65

[18] T.H. Nguyen, Q.A.D. Le, H.P.A. Nguyen, and M.H. Do, Anal. Bioanal. Electrochem. 17 (2025) 18.
[19] QD-BKHCN, TCVN 9745-1:2013.
[20] K. Neubauer, ICP-OES and ICP-MS Techniques for Today's Spectroscopists 38 (2023) 6.
[21] T. Atomssa, and A.V. Gholap, J. Eng. Tech. 7 (2015) 22.
[22] N.H. Md Said, K. Boon, and P. Sharma, J. Mater. Chem. A 1892 (2017) 150002.
[23] N. Vasanthi Sridharan, and B.K. Mandal, ACS Omega 7 (2022) 45469.
[24] A. Afkhami, M. Fathi, and H. Sohrabi, Anal. Chim. Acta 771 (2013) 21.
[25] A. Kawde, T. Choi, and Y. Kim, Microporous Mesoporous Mater. 243 (2017) 1.
[26] A Statistical Overview of Standard (Iupac And Acs) and New Procedures for Determining the Limits of Detection and Quantification: Application to Voltammetric and Stripping Techniques (2004).
[27] N.Y. Stozhko, L. Petrosyan, and D. Boychenko, J. Solid State Electrochem. 12 (2008) 1185.
[28] V.S. Somerset, E.I. H., and I. Iwuoha, J. Environ. Sci. Health A 46 (2011) 17.
[29] Y. Hao, X. Liu, and S. Li, J. Electrochem. Soc. 168 (2021) 083503.
[30] E.W. Nunes, M.K.L. Silva, and I. Cesarino, Chemosensors 8 (2020) 53.
[31] G.K. Ramesha, S. K. Prasad, and K. L. Prasad, J. Colloid Interface Sci. 361 (2011) 270.
[32] F. Liu, W. Zhu, and Y. Li, ACS Appl. Mater. Interfaces 4 (2012) 922.